

# Complex formation, rearrangement, and reaction in $\text{PhOH}^+ + \text{ND}_3$ : Vibrational mode effects, recoil velocities, and *ab initio* studies

Richard J. Green, Ho-Tae Kim, Jun Qian, and Scott L. Anderson  
*Department of Chemistry, University of Utah, Salt Lake City, Utah 84112-0850*

(Received 22 May 2000; accepted 16 June 2000)

Vibrationally mode-selected phenol cations ( $\text{C}_6\text{H}_5\text{OH}^+$  and  $\text{C}_6\text{D}_5\text{OH}^+$ ) were reacted with  $\text{ND}_3$  in a guided-ion-beam instrument. Integral cross sections and recoil velocity distributions are reported as a function of collision energy and vibrational state. Three reactions are observed. A small signal is found for the  $[\text{PhOH}:\text{ND}_3]^+$  adduct at low total energies, indicating the formation of a very long-lived complex. The major reaction is H/D exchange, generating  $\text{PhOD}^+ + \text{ND}_2\text{H}$ . Exchange is  $\sim 40\%$  efficient at low energies, strongly inhibited by collision energy, and strongly enhanced by excitation of  $\text{PhOH}^+$  vibrations. Recoil velocity distributions suggest that H/D exchange proceeds through a statistical complex at all energies. A precursor complex is invoked to explain the energy and vibrational state dependence. The endoergic proton transfer reaction is a minor channel at all energies, with dynamics intermediate between the direct and complex limits. Quantum chemistry and RRKM calculations are reported, providing an additional mechanistic insight. © 2000 American Institute of Physics. [S0021-9606(00)01634-2]

## I. INTRODUCTION

Reactions of even small polyatomic ions with small molecules can be rather complex, with multiple product channels and multiple potential wells and transition states controlling motion on the potential energy surface. Because dynamics calculations on such complicated surfaces are generally infeasible, experimental tools must have sufficient sensitivity to the important dynamical effects, but must also yield results that are interpretable. We have found that a combination of measuring the effects of reactant vibrational excitation and collision energy, together with measurements of product recoil velocity distributions, provides considerable insight into reaction mechanisms.<sup>1,2</sup> Vibrational effects tend to probe events early along the reaction coordinate, providing insight into the nature of rate-limiting transition states. Varying collision energy allows us to vary the available energy over a wide range, and also control collision time scale. Recoil velocity distributions probe collision time scales, the degree of energy randomization, the preferred scattering mechanisms, and the possible presence of barriers in the exit channel. When combined with isotope labeling experiments and *ab initio* calculations of complexes, transition states, and unimolecular kinetics, a fairly complete reaction mechanism can be constructed.

Here we report a study of this type on the reaction of phenol cations with ammonia, where the vibrational state of  $\text{PhOH}^+$  is controlled using mass-analyzed threshold ionization. This system is a prototypical acid-base combination, is expected to form hydrogen-bonded complexes, and may allow formation of ring-coordination complexes as well. It is also considerably more complex than previous systems for which detailed vibrationally-mode-selected scattering has been reported. The exception is our recent study of the  $\text{PhOH}^+$  reaction with methylamine,<sup>3</sup> although in that system

the chemistry is much simpler, and as a result, less mechanistic insight was obtained.

One purpose for this study was to see what sorts of vibrational effects might be found in larger systems. For a number of reasons, we did not expect large effects. Problems with IVR in the ionization process make it impossible to produce  $\text{PhOH}^+$  (or any large cation?) with excitation in high frequency vibrations. In particular, we are not able to produce  $\text{PhOH}^+$  with OH stretching or bending excitation. Here we report on the effect of two low-frequency in-plane ring modes, neither of which is obviously coupled to the reaction coordinate. For a system with 45 vibrational degrees of freedom, excitation of low frequency modes is not expected to have large effects, although even small mode-specific effects are very helpful in developing a reaction mechanism.<sup>4-6</sup> The biggest surprise in the present study is that large (factor of two) effects are observed, demonstrating that even low frequency modes can strongly influence dynamics.

By combining the experimental results with electronic structure and RRKM calculations, we are able to develop a detailed mechanism for how the scattering/reaction dynamics change with energy. At least two distinct types of intermediate complexes are important in mediating reaction, and product branching is determined by competition between direct reaction, trapping into complexes, and isomerization between complexes. The largest vibrational effect is tentatively attributed to an enhancement of the isomerization probability from ring-coordinated to hydrogen-bonded complexes.

## II. EXPERIMENTAL METHODOLOGY

The guided-ion beam instrument and methodology used in this study have been described previously.<sup>7,8</sup> Vibrationally state-selected beams of  $\text{PhOH}^+$  were prepared by mass-analyzed threshold ionization<sup>9</sup> of a pulsed beam of phenol

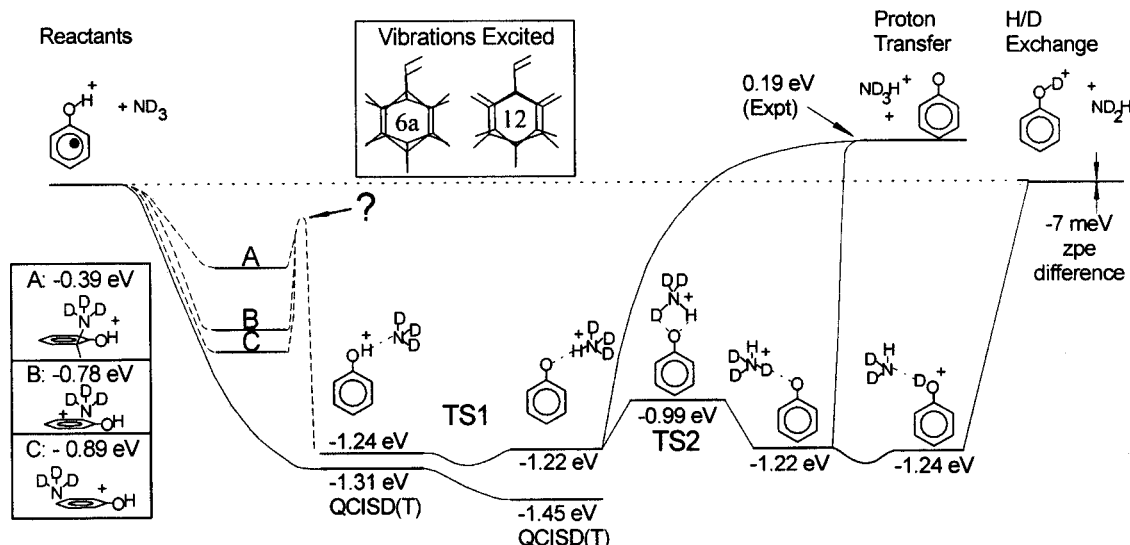


FIG. 1. Reaction coordinate diagram for PhOH<sup>+</sup>+ND<sub>3</sub>. Except as indicated the energies are calculated from differences in MP2/6-31G\* calculations. Some results extracted from a series of QCISD(T)/6-31G\* and G3 calculations are also shown. For proton transfer, we give our experimental endoergicity. The heavy dot superimposed on the PhOH<sup>+</sup> reactant structure shows the center of charge. The inset shows the extrema of vibrational trajectories for the two vibrations excited.

seeded in helium. Phenol was single-photon excited to a particular vibrational level of the <sup>1</sup>L<sub>b</sub>(S<sub>1</sub>) state, then excited by a second laser to high Rydberg states converging on the same vibration in the cation. Both laser wavelengths were generated using a single Nd:YAG laser to pump a pair of dye lasers, using appropriate frequency up-conversion to generate tunable UV.

Prompt ions created by REMPI, autoionization, or other processes were separated from the state-selected Rydberg molecules by a weak retarding field (~3 V/cm). The Rydberg molecules were then field-ionized by a 30 V/cm pulse, creating a beam of state-selected reactant ions. The ion beam was injected into a quadrupole ion guide where time-of-flight (TOF) gating was used to sharpen the temporal and energy widths of the beam pulse. The pulse (~15 μs wide) was then injected into a system of octapole ion guides. The first segment of the octapole guided the reactant ions through a scattering cell containing ND<sub>3</sub> (Cambridge Isotope Labs, 99 at %), where a small fraction of the ions could react. Product ions, together with unreacted PhOH<sup>+</sup>, were collected by the ion guide and passed into a second, longer segment of the octapole guide system. Velocity distributions of both reactants and products were measured by TOF in the guides. Finally, the ions were mass-analyzed and detected. ND<sub>3</sub> pressure was adjusted to maintain single collision conditions, as shown by pressure-independence of the measured cross sections and branching ratios.

### III. RESULTS

A series of *ab initio* calculations<sup>10</sup> on this system were reported in our paper on the energetics of proton transfer in PhOH<sup>+</sup>+ND<sub>3</sub>.<sup>11</sup> Those results are summarized in Fig. 1, together with additional calculations on non-hydrogen-bonded complexes. For the hydrogen-bonded complexes, our results are generally in good agreement with the MP2 calculations of Yi *et al.*<sup>12</sup> For the proton transfer (PT) reaction we give

our experimental value for the PT endoergicity.<sup>11</sup> For the H/D exchange reaction the exoergicity is based on zero point calculations at the MP2/6-31G\* level. A number of complexes were located, and geometries were optimized with both MP2/6-31G\* and B3LYP/6-31G\* theories, with similar structures resulting. Single point QCISD(T)/6-31G\* calculations were done at both MP2 and B3LYP geometries, and the QCISD(T) results shown are for whichever geometry gave the lowest energy. All energetics include scaled<sup>13</sup> zero point energy corrections appropriate to [PhOH-ND<sub>3</sub>]<sup>+</sup>. The transition state for intracomplex proton transfer (TS1) was optimized at both B3LYP and MP2 levels. With B3LYP, there is no barrier to the [PhOH-ND<sub>3</sub>]<sup>+</sup> → [PhO-HND<sub>3</sub>]<sup>+</sup> transformation. At the MP2 level there is a small barrier that disappears when zero-point energy is included. A QCISD(T) single point at the MP2-optimized TS1 structure also shows no signs of a barrier when zero-point energy corrected. The other important transition state found is the C<sub>2v</sub> structure, TS2. This, as far as we can determine, is the lowest energy TS for H/D exchange, and is probably rate-limiting. To check that multiple configurations were not a problem, particularly at transition structures, CASSCF(3,6)/6-31G\* single points were performed for the hydrogen-bonded complexes and transition structures. The Hartree-Fock configuration was found to account for >97% of the active space.

In addition to the hydrogen-bonded complexes, several non-hydrogen-bonded complexes were found (A-C in Fig. 1). The two most stable (B and C) have ND<sub>3</sub> oriented so that the nitrogen lone pair is perpendicular to the phenyl ring plane, directed approximately toward the midpoint of the ortho or para CH bonds, with the closest approach between ND<sub>3</sub> and PhOH moieties being 2.29 Å and 2.39 Å, respectively, for the ortho and para complexes. The affected carbon atom is slightly displaced from the ring plane toward ND<sub>3</sub>, and the hydrogen atom is displaced away from ND<sub>3</sub>. Complex A is similar to the ortho coordination complex, except

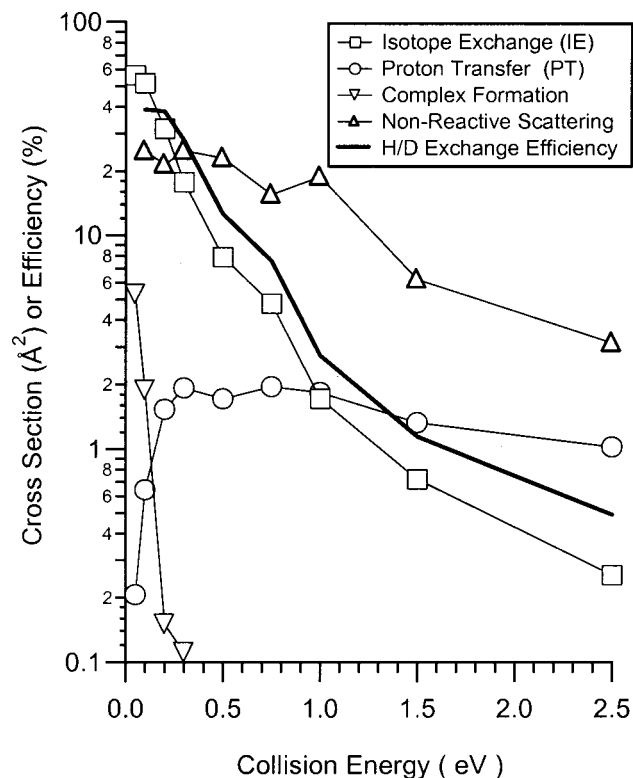


FIG. 2. Data Points: Measured cross sections for reaction of ground state  $\text{PhOH}^+$  with  $\text{ND}_3$ . Solid curve: Estimated efficiency for the H/D exchange reaction.

that the  $\text{D}_3\text{N}-\text{C}$  distance has decreased to 1.56 Å, corresponding to a covalent bond, and the H atom attached to the ortho carbon is shifted so that the CH bond angle with respect to the ring plane is  $46^\circ$ . The binding energy in this covalently bound complex is substantially weaker than in the coordination complexes. Because these complexes are very slow to optimize, we have not attempted a complete search, nor have we attempted to find transition states for interconversion.

To give some idea of the types of vibrational motion probed, the inset to Fig. 1 shows superimposed extrema for the vibrational trajectories of the two modes excited. The experimental frequencies for the two modes are  $516\text{ cm}^{-1}$  and  $815\text{ cm}^{-1}$ , respectively. The normal modes for  $\text{PhOH}^+$  were calculated with Hartree-Fock, MP2 and B3LYP with varying basis sets. B3LYP/6-311+G\*\* gave the best match with the experimental frequencies ( $526$  vs  $516$  and  $818$  vs  $815\text{ cm}^{-1}$ ), and normal modes from that calculation are plotted, using gOpenMol to visualize the vibrations.<sup>14</sup> The modes are assigned as the  $x$ -sensitive  $\nu_{6a}$  and  $\nu_{12}$  vibrations.<sup>15</sup> Note that neither mode involves OH stretching.  $\nu_{6a}$  involves collective motion of the COH moiety, with little change in CO bond length or COH bond angle.  $\nu_{12}$  also preserves the COH angle, but has significant CO stretching character.

Finally, calculations of atom charges and the center-of-charge for the  $\text{PhOH}^+$  reactant were carried out using the CHelpG scheme<sup>16</sup> at the MP2/6-31G\* level. CHelpG calculations were done both for the equilibrium geometry and for  $\text{PhOH}^+$  distorted along the vibrational normal coordinates.

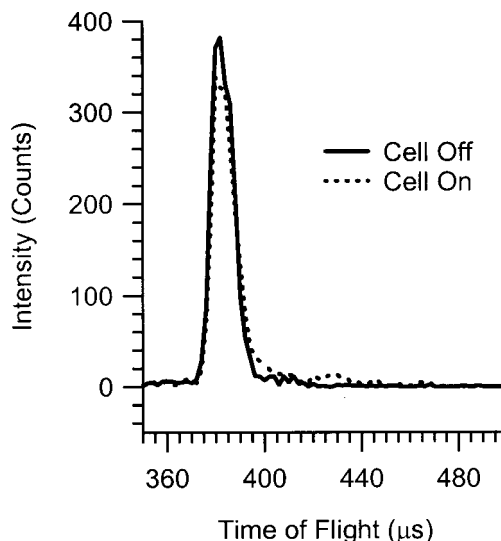


FIG. 3. Time of flight for  $\text{PhOH}^+$  ions with scattering cell filled or empty of  $\text{ND}_3$ , showing inelastic scattering.

The center-of-charge is located near the center of the phenyl ring, as indicated by a heavy dot plotted on the reactant  $\text{PhOH}^+$  structure in Fig. 1.

### A. Integral cross sections

The absolute cross sections for reaction of  $\text{C}_6\text{H}_5\text{OH}^+$  with  $\text{ND}_3$  are shown in Fig. 2. The dominant channel at low energies is production of  $\text{PhOD}^+$ , via isotope exchange. Also shown as a solid curve is the percent efficiency of the H/D exchange reaction, i.e., the ratio of the experimental cross section to the collision cross section. The collision cross section is taken as the greater of the capture cross section or the hard sphere cross section ( $\sim 63\text{ Å}^2$ ). The capture cross section is estimated using the statistical adiabatic channel model of Troe.<sup>17</sup> The efficiency is around 40% at low collision energy, but drops rapidly to less than a few percent above 1 eV. The hard sphere cross section was estimated using the calculated geometries for  $\text{PhOH}^+$  and  $\text{ND}_3$ , with appropriate angle averaging.

Proton transfer is a minor channel with a clear threshold and best-fit endoergicity of  $\sim 0.195\text{ eV}$ .<sup>1</sup> Even at collision energies well above the endoergicity, proton transfer occurs in no more than a few percent of collisions.

A minor, but mechanistically important product is the collision adduct  $[\text{PhOH}-\text{ND}_3]^+$ . The cross section in this case is really an effective cross section for forming, then detecting the adduct. The significant cross section implies that the adduct lifetime is long enough that some fraction survives to be detected. The adducts have a well defined velocity ( $V_{\text{CM}}$ , the velocity of the center of mass relative to the lab) and thus, a well defined flight time to the detector ( $\sim 1\text{ ms}$ ). Either the adduct lifetime is long enough to allow some survival probability, or survival is enhanced via radiative or collisional stabilization. The spontaneous IR emission timescale is almost certainly too long to allow significant radiative cooling during the 1 ms flight time. At the scattering cell pressures used, however, the time between collisions is  $\sim 300\text{ μs}$ , thus collisional stabilization is possible. Note,

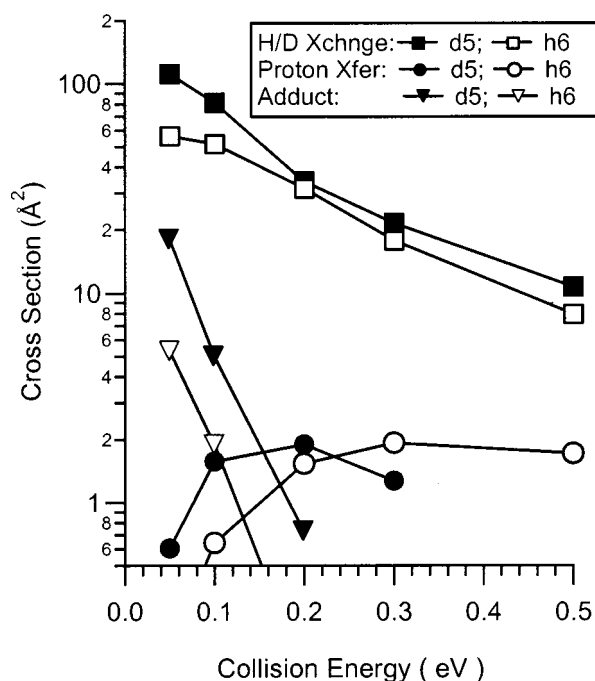


FIG. 4. Comparison of cross sections for reaction of ground state C<sub>6</sub>H<sub>5</sub>OH<sup>+</sup> and C<sub>6</sub>D<sub>5</sub>OH<sup>+</sup> with ND<sub>3</sub>.

however, that the average time spent in the cell is only  $\sim 100$   $\mu$ s, thus only a fraction of the adduct products experience a secondary collision, regardless of lifetime. In any case, it is clear that adducts must form with reasonable efficiency in low energy PhOH<sup>+</sup>-ND<sub>3</sub> collisions, and that their lifetimes must be in the tens of microseconds range. As expected, the effective cross section for detecting the adduct declines rapidly with increasing collision energy as the lifetime drops below the range where survival or stabilization are possible.

The final cross section shown is for a particular subset of non-reactive scattering events. This cross section has been estimated by examining the effects of scattering on the velocity distributions of the PhOH<sup>+</sup> primary ions. With the scattering cell empty, the PhOH<sup>+</sup> beam has a sharp velocity distribution. When filled, the sharp peak in the distribution is attenuated by a combination of reactive and nonreactive scattering. The reactive scattering results in net loss of signal from the primary beam TOF spectrum. Non-reactive scattering results in appearance of a distribution of slower ions, as shown in Fig. 3, which gives typical PhOH<sup>+</sup> velocity distributions recorded with and without ND<sub>3</sub>. We are interested in that fraction of collisions that form a collision complex, but then decay back to reactants. In such collisions, low recoil velocities are expected, thus to capture these events we integrate the nonreactive signal only over the velocity range near  $V_{CM}$ .

Figure 4 compares the cross sections for reaction of *d*<sub>5</sub>-PhOH<sup>+</sup>(C<sub>6</sub>D<sub>5</sub>OH<sup>+</sup>) with those for *h*<sub>6</sub>-PhOH<sup>+</sup> over the low collision energy range where they differ significantly. There are several points of interest. There is no ND<sub>4</sub><sup>+</sup> product detected, nor do we observe the decrease in the H/D exchange cross section that would be expected if the ring hydrogen atoms were involved in the atom exchange process.

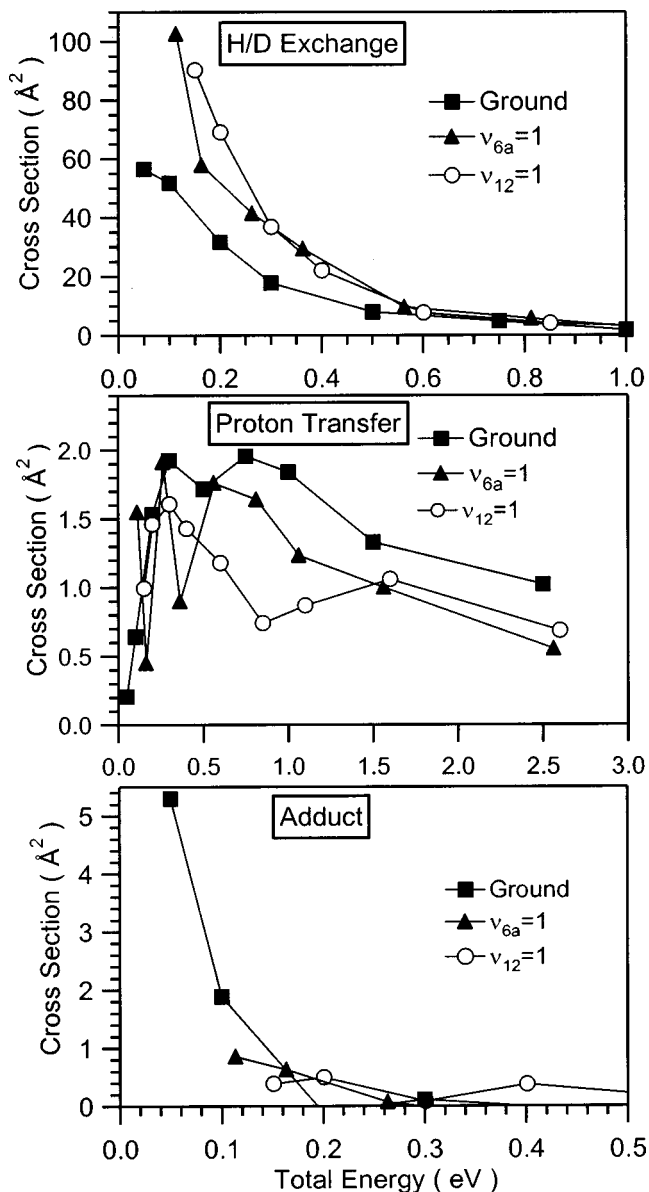


FIG. 5. Cross sections for reaction of PhOH<sup>+</sup> in different vibrational states with ND<sub>3</sub>, plotted as a function of total energy (=collision+vibration).

Lack of activity for the ring hydrogen atoms is expected; they are substantially more strongly bound.<sup>11</sup> The other major point is that in the energy range below  $\sim 0.2$  eV, the *d*<sub>5</sub>-PhOH<sup>+</sup> cross sections are uniformly higher than the equivalent *h*<sub>6</sub>-PhOH<sup>+</sup> values. The difference is largest for the adduct channel, where the effective cross section increases by a factor of  $\sim 4$  upon deuteration of the ring. The H/D exchange cross section increases by a factor of  $\sim 2$ , and the proton transfer cross section increases by a factor of  $\sim 2.5$ .

Figure 5 shows the effects of PhOH<sup>+</sup> vibration on the cross sections. Note that the cross sections are plotted for different energy ranges and are plotted as a function of total energy (collision plus vibrational energy) in order to allow direct comparison of the effects of vibration and collision energy. The effective cross section for adduct formation/survival (bottom frame) appears to vary primarily with total energy. The H/D exchange reaction is strongly inhibited by

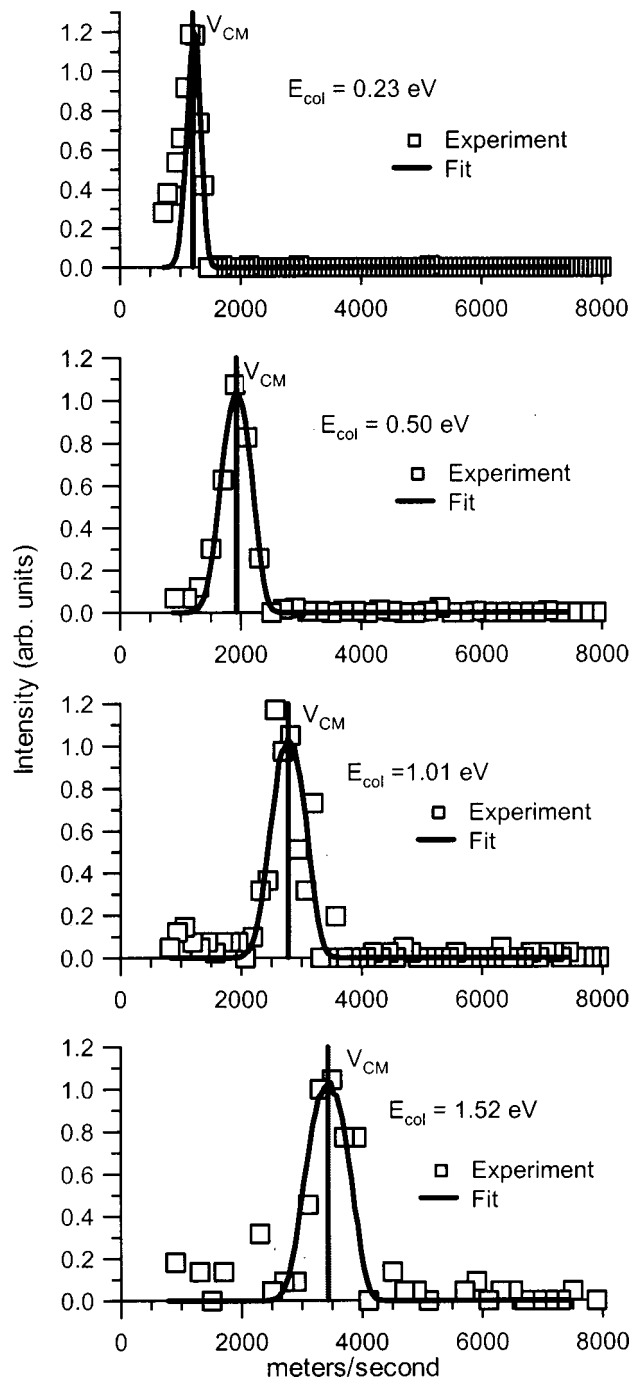


FIG. 6. Axial lab frame velocity distributions for the  $\text{PhOD}^+$  product from H/D exchange at three collision energies.  $V_{\text{CM}}$  is the velocity of the center-of-mass frame in the lab.

collision energy but strongly enhanced by both  $v_{6a}$  and  $v_{12}$  vibrations. The enhancement is slightly greater on a per energy basis for  $v_{12}$  than for  $v_{6a}$ , and neither vibration has a significant effect at energies above  $\sim 0.5$  eV. For the endoergic proton transfer reaction, both vibration and collision energy provide similar enhancements in the threshold energy range, but there is a weak, but reproducible, vibrational inhibition at high energies.

## B. Product velocity distributions

Time of flight (TOF) was used to record axial velocity distributions for reactants and products, as described

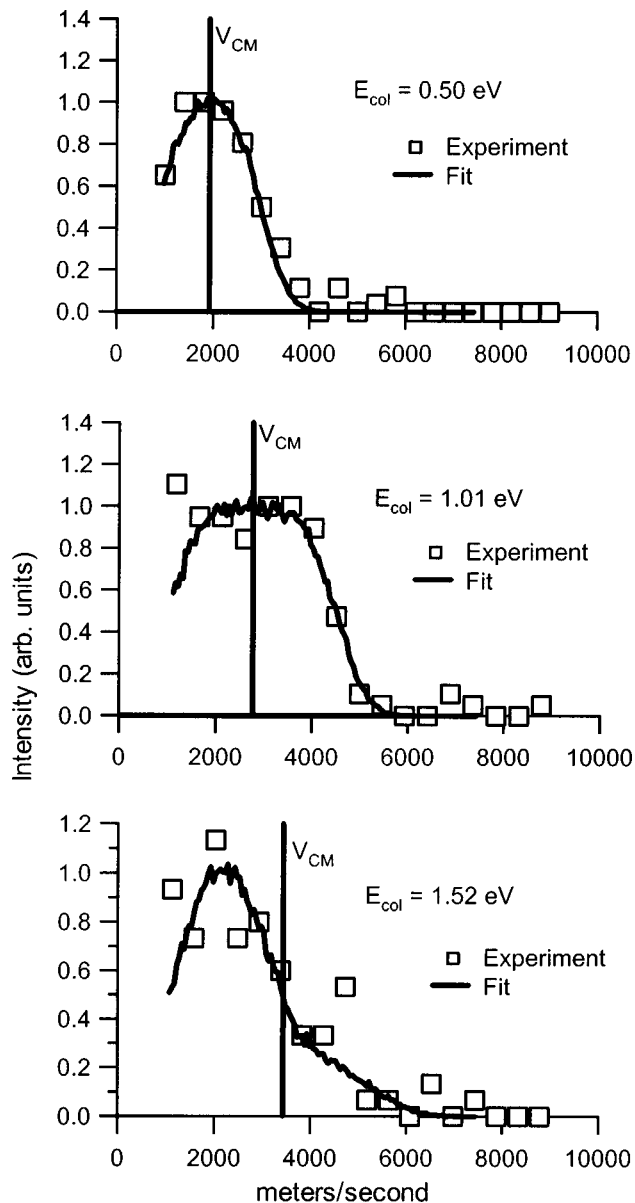


FIG. 7. Axial lab frame velocity distributions for the  $\text{ND}_3\text{H}^+$  product from proton transfer at four collision energies.  $V_{\text{CM}}$  is the velocity of the center-of-mass frame in the lab.

previously.<sup>7</sup> Axial velocity distributions are simply the projection of the full velocity distribution on the octapole guide axis, which is co-axial with the average relative velocity vector ( $\langle v_{\text{rel}} \rangle$ ) and the average  $V_{\text{CM}}$ . Two pieces of information can be read directly from the distributions. If reaction proceeds via a collision intermediate with lifetime long compared to its rotational period, the resulting axial velocity distributions must be forward-backward symmetric about  $V_{\text{CM}}$  (forward is defined as faster than  $V_{\text{CM}}$ ). Conversely, an asymmetric distribution implies a direct reaction where the collision time is short. The maximum deviation of the axial velocity distribution from  $V_{\text{CM}}$  is a measure of the maximum energy going into recoil of the products. One caveat is that the apparent velocities of product ions with low lab energies are easily distorted by surface potentials on the octapole. For this reason, the reported distributions are truncated at velocities corresponding to  $\sim 100$  meV.

TABLE I. Summary of recoil velocity distribution fits.

Reaction	Collision energy (eV)	$L_{\text{avg}}$ ( $\hbar$ )	$\tau_{\text{complex}}$	$\langle E_{\text{recoil}} \rangle$ (eV)	$\langle E_{\text{recoil}} \rangle / \langle E_{\text{avail}} \rangle$
H/D					
Exchange	0.12	133	>2.2 ps	<0.01	~6%
	0.22	146	>2.5 ps	<0.03	~11%
	0.50	170	>1.8 ps	0.15	~27%
	1.01	196	>1.5 ps	0.32	~30%
	1.52	214	>1.4 ps	0.49	~31%
Proton					
Transfer	0.50	170	>1.8 ps	0.17	43%
	1.01	196	>1.5 ps	0.33	38%
	1.52	214	300 fs	0.51	37%

Axial velocity distributions for the H/D exchange product from reaction of ground state PhOH<sup>+</sup> at selected energies are shown in Fig. 6. At all collision energies ( $E_{\text{col}}$ ) the distributions are symmetric about  $V_{\text{CM}}$ , within experimental error, but the width of the distributions increases with increasing energy. Results for the proton transfer reaction are given in Fig. 7. For PT, the distributions are noisy because of the small cross section, but appear forward–backward symmetric for energies up to about 1 eV, then distinctly backward peaked at higher energies. The width of the distributions increases substantially with collision energy. Distributions were measured for reaction of vibrationally excited PhOH<sup>+</sup> as well, but are not plotted as they do not differ significantly from those for the ground state. Negligible vibrational effect on recoil velocities is typical of systems we have studied.<sup>4–8</sup> Recoil behavior is most sensitive to dynamics late in the collision, by which time the reactant vibration excitation is scrambled. The energy contributed by reactant vibration is simply too small to significantly affect recoil.

The osculating complex model of Fisk *et al.*<sup>18</sup> was developed to treat angular distributions in the transition between direct and complex-mediated mechanisms. By fitting the experimental distributions to this model, we can correct for experimental broadening factors (reactant velocity distributions) and extract estimates for both collision time and the  $E_{\text{recoil}}$  distribution.<sup>7</sup> The model assumes that reaction is mediated by a complex that decomposes to products unimolecularly with lifetime,  $\tau_{\text{complex}}$ . The complex also rotates, with classical period,  $\tau_{\text{rot}}$  determined by its moment of inertia and the available angular momentum ( $L$ ).  $\tau_{\text{rot}}$  is calculated using moments of inertia from the *ab initio* calculations, and  $L_{\text{avg}}$ , corresponding to the average impact parameter leading to capture, estimated using the statistical adiabatic channel theory.<sup>17</sup> For the PhOH<sup>+</sup>–ND<sub>3</sub> system,  $\tau_{\text{rot}}$  drops smoothly from ~4.4 ps at  $E_{\text{collision}}=0.1$  eV to ~1.8 ps at 2 eV. As  $\tau_{\text{complex}}$  drops below ~0.5 $\tau_{\text{rot}}$ , the velocity distributions become progressively asymmetric, providing a signature for decreasing collision time. In our fitting, the  $P(E_{\text{recoil}})$  distribution is assumed to be a Gaussian, peaking at  $f_{\text{peak}} \cdot E_{\text{avail}}$  with width =  $f_{\text{width}}/E_{\text{avail}}$ ,

$$P(E_{\text{recoil}}) = \exp \left[ - \left( \frac{f_{\text{width}} \cdot [E_{\text{recoil}} - f_{\text{peak}} \cdot E_{\text{avail}}]}{E_{\text{avail}}} \right)^2 \right].$$

TABLE II. Collision time scales.

Collision energy	Hydrogen-bonded RRKM <sup>a</sup>	Para-ring-bonded RRKM <sup>a</sup>	Direct collision time <sup>b</sup>
0.1 eV	4 $\mu$ s	2 ns	0.46 ps
0.5 eV	1 ns	1.3 ps	0.21 ps
0.8 eV	70 ps	0.16 ps	0.16 ps
1.0 eV	20 ps	<100 fs <sup>c</sup>	0.15 ps
1.5 eV	1.6 ps	<100 fs <sup>c</sup>	0.12 ps
2.0 eV	0.3 ps	<100 fs <sup>c</sup>	0.10 ps

<sup>a</sup>For  $L=L_{\text{avg}}$ .

<sup>b</sup>Time for reactants to traverse 5 Å.

<sup>c</sup>Lifetime below limit where RRKM is expected to be valid.

$E_{\text{avail}}$  is the total available energy in the products, i.e., the sum of  $E_{\text{collision}}$ , the reaction exoergicity and the reactant vibrational and rotational energies.  $E_{\text{vibration}}$  depends on the state selected, and  $E_{\text{rotation}}$  is a thermal distribution at the scattering cell temperature (~350 K). The model depends on only three parameters ( $\tau_{\text{complex}}$ ,  $f_{\text{width}}$ ,  $f_{\text{peak}}$ ), all of which are physically significant. Fitting is done with a Monte Carlo simulation of the experiment, discussed previously.<sup>7</sup>

The results of osculating complex fits to the velocity distributions are given in Table I. Note that for the H/D exchange channel, the kinematics are such that the total recoil velocity is partitioned primarily to the light neutral product, rather than the detected ion. As a result, the velocity resolution is poor, particularly at low collision energies where much of the width of the distribution results from ion beam and target velocity distributions. The average recoil energy ( $\langle E_{\text{recoil}} \rangle$ ) extracted from the modeling has high uncertainty, as does the fraction of available energy going into recoil ( $\langle E_{\text{recoil}} \rangle / \langle E_{\text{avail}} \rangle$ ). At low collision energies we can only say that the fraction of available energy going to recoil is small, but there appears to be a significant increase at the highest energies.

For the proton transfer reaction, the kinematics are more favorable, and there are several significant differences compared to the H/D exchange channel. First, it is obvious that at high energies, the PT products are backward peaked with respect to  $V_{\text{CM}}$ , indicating dominance of a direct reaction mechanism, i.e., a collision time short compared to  $\tau_{\text{rot}}$ . At lower energies the distributions are forward–backward symmetric, however, the fraction of available energy appearing in recoil ( $\langle E_{\text{recoil}} \rangle / \langle E_{\text{avail}} \rangle$ ) remains large.

## IV. DISCUSSION

### A. Adduct

The first question to address is whether observation of the collision adduct is consistent with the *ab initio* energetics. As noted, this observation implies that some fraction of the adducts must survive to be detected or collisionally stabilized, in either case implying a lifetime in the tens of microsecond range, at least. We have estimated the lifetime as a function of energy using the RRKM program of Zhu and Hase,<sup>19</sup> using its direct state count algorithm, scaled<sup>13</sup> frequencies from our MP2 calculations, and our QCISD(T) energetics. The results are summarized in Table II. Lifetimes

are reported for complexes with the average angular momentum for capture ( $L_{\text{avg}}$ ). For comparison purposes we have calculated lifetimes for the most stable hydrogen-bonded and non-hydrogen-bonded geometries ( $[\text{PhO}-\text{ND}_3\text{H}]^+$  and complex C, Fig. 1, respectively). For the hydrogen-bonded complex, all three exit channels are included:  $\text{PhOH}^+ + \text{ND}_3$ ,  $\text{PhOD}^+ + \text{ND}_2\text{H}$ , and  $\text{PhO} + \text{ND}_3\text{H}^+$ . Note that the branching to the endoergic proton transfer products ( $\text{PhO} + \text{ND}_3\text{H}^+$ ) is less than a few percent over the energy range of interest. The details of the non-hydrogen-bonded calculation are given in the next section.

Only the hydrogen-bonded complex is stable enough to account for the observed adduct. For our lowest collision energy (0.05 eV), the lifetime for a complex with  $L_{\text{avg}}$  is 18  $\mu\text{s}$ , dropping rapidly for increasing collision energy. In comparing with experiment, it is important to note that there is a distribution of collision energies at each experimental energy, resulting from ion beam energy spread and target motion. The standard deviation of the  $E_{\text{collision}}$  distribution at low collision energies is  $\sim 0.1$  eV. At nominal energies of 0.05 and 0.1 eV, therefore, a significant fraction of collisions are at very low energies, resulting in complexes with the long lifetimes required for direct detection or collisional stabilization. For higher energies, the fraction of collisions with energies low enough to result in detectable adducts drops rapidly.

The other interesting observation along these lines is that the effective cross section for adduct formation/detection increases by a factor of about 4 in reaction to  $d_5\text{-PhOH}^+$ . This enhancement also appears to be consistent with the RRKM modeling, where it is found that because of a higher density of states in the complex, the lifetime of  $[d_5\text{-PhOH}-\text{ND}_3]^+$  adducts are 6–8 times longer than those of  $[h_6\text{-PhOH}-\text{ND}_3]^+$  at the same energy.

In principle, we could use a RRKM-based fit to the adduct cross section to provide an experimental value for the adduct binding energy. We have not done this because there are too many uncertainties, including the adduct formation cross section (and its dependence on  $E_{\text{collision}}$  and  $L$ ) and the detailed experimental collision energy distribution at very low nominal energies. Nonetheless, it is clear that the adduct binding energy must be close to the QCISD(T) result (1.45 eV) for the hydrogen-bonded complex. For example, if we assume a binding energy equal to the MP2/6-31G\* value (1.24 eV), the RRKM lifetimes are about 12 times shorter, and we would not detect significant adduct signal. Conversely, significantly stronger binding would result in detection of adducts at energies higher than observed. In any case, it is clear that the non-hydrogen-bonded complexes (A–C in Fig. 1), are not nearly stable enough to account for the adduct signal.

## B. H/D exchange mechanism

H/D exchange, because it requires at least two bonds to break and reform, almost certainly requires a long-lived collision complex. The fact that the axial velocity distributions are forward–backward symmetric at all energies is consistent with this requirement, as is the observation that the fraction of available energy appearing as recoil energy of the prod-

ucts is small. Other observations that must be accounted for are the observed strong inhibition by collision energy, the enhancement produced by vibrational excitation, and the enhancement from ring-deuteration.

A plausible low energy reaction path, based on our ab initio calculations, is shown in Fig. 1. Reactants can form a hydrogen-bonded  $[\text{PhOH}-\text{ND}_3]^+$  complex, and there is clearly no barrier to this association process, as shown by observation of the hydrogen-bonded adduct at low energies. In this complex, the available internal energy ( $= E_{\text{collision}} + E_{\text{vibration}} + E_{\text{rotation}} + \text{well depth}$ ) is far in excess of the barrier (if any) to intracomplex proton transfer (TS1), and this transition state is relatively loose. It is reasonable to conclude, therefore, that isomerization between the  $[\text{PhOH}-\text{ND}_3]^+$  and  $[\text{PhO}-\text{HND}_3]^+$  forms of the complex is rapid compared to the long complex lifetime, and that much of the time is spent in the energetically more-favorable  $[\text{PhO}-\text{HND}_3]^+$  configuration. While in this configuration, it is possible for the  $\text{NHD}_3$  moiety to flip through TS2, thus accomplishing H/D exchange. Following exchange, the rapid intracomplex proton (deuteron) transfer process will establish a population of  $[\text{PhOD}-\text{ND}_2\text{H}]^+$ , and if the complex dissociates while in the  $[\text{PhOD}-\text{ND}_2\text{H}]^+$  form, H/D exchange products result. Note that in this mechanism, there is no exchange of phenyl ring H atoms, in agreement with experiment.

In this mechanism, the degree of isotope scrambling is determined by the rate of passage through TS2 relative to the lifetime of the complex with respect to dissociation. RRKM analysis indicates that at our lowest collision energies, the TS2 passage rate is in the  $10^{11} \text{ s}^{-1}$  range, compared to complex lifetimes in the microsecond range. At low collision energies, then, complete scrambling is expected. The dissociation rate of the complex increases more rapidly with increasing energy than the TS2 passage rate, however, so that at energies above  $\sim 1.3$  eV scrambling should become increasingly incomplete (the dissociation and TS2 passage rates are equal at  $E_{\text{col}} \approx 1.8$  eV).

Because the group of scrambled atoms includes one H and three D atoms, the observed H/D exchange cross section should be  $\sim 75\%$  of the cross section for formation of the hydrogen-bonded complex, at least for  $E_{\text{col}} < \sim 1.3$  eV. Actually, because zero point energy favors  $\text{PhOD}^+ + \text{ND}_2\text{H}$  by  $\sim 7$  meV (Fig. 1), RRKM analysis predicts that H/D exchange should occur in 76%–85% of collisions in which the hydrogen-bonded complex is formed (the higher probability being at low energies). In Fig. 2 we plot the efficiency of H/D exchange as a fraction of total collisions ( $\sigma_{\text{exchange}}/\sigma_{\text{collision}}$ ). At  $E_{\text{collision}} = 0.2$  eV the efficiency is about 40%, dropping to  $< 1\%$  at high energies. Given that the branching out of the hydrogen-bonded complex should give  $\sim 80\%$  H/D exchange, 40% net H/D exchange efficiency implies that such complexes form in only about 50% of collisions at low energies, and that hydrogen-bonded complex formation is strongly inhibited by collision energy.

For  $d_5\text{-PhOH}^+$ , the H/D exchange cross section is nearly doubled at low collision energies (Fig. 4). As noted above, ring deuteration does increase the lifetime of the hydrogen-bonded complex, however, this effect cannot ex-

TABLE III. Single point energies for various ND<sub>3</sub>-hydroxyl orientations.

Geometry	Energy with respect to reactants	
	2 Å separation	2.3 Å separation
LP over H	0.23	0.04
LP over O	1.69	0.50
LP over C	0.64	0.11
Flipped over H	0.80	0.58
Flipped over O	1.68	1.03
Flipped over C	1.31	0.70
Out-of-plane NH-O	0.34	0.32
In-plane NH-O	0.39	0.28
Stretch	-0.92	-0.64
Rotate 35°	-0.62	-0.52

plain the doubling because even for  $h_6$ -PhOH<sup>+</sup>, the hydrogen-bonded complexes live far longer than required for H/D scrambling at low energies. The conclusion is that ring-deuteration nearly doubles, to ~100%, the probability for forming the hydrogen-bonded complex in low energy collisions. Similarly, excitation of the  $\nu_{6a}$  and  $\nu_{12}$  PhOH<sup>+</sup>, vibrations leads to a substantial increase in H/D exchange. In this case it is clear that the enhancement must result from increased efficiency of forming the hydrogen-bonded complex, rather than some effect of vibration on the chemistry following complex formation. This conclusion rests on the idea that energy is rapidly randomized in such strongly bound complexes. In order for vibration and collision energy to have opposite effects, the rate-limiting step must occur prior to complex formation.

To account for these effects we propose a precursor complex mechanism, in which H/D exchange occurs via two pathways. At all energies, collisions in “ND<sub>3</sub> on hydroxyl” geometries can access the hydrogen-bonded complexes needed for H/D exchange. Given both the shape and center-of-charge (Fig. 1) of PhOH<sup>+</sup>, it is clear, however, that most collisions are in “ND<sub>3</sub> on ring” geometries. We propose that at low collision energies, these “ND<sub>3</sub> on ring” collisions have high probability for trapping into ring-bound, precursor complexes (Fig. 1, A–C), with the subsequent possibility of transition to the reactive hydrogen-bonded geometry.

For H/D exchange to occur in collisions that initially form ring-coordinated complexes, there must be a transition to the hydrogen-bonded geometry. The barrier, or barriers, separating ring-bound and hydrogen-bonded geometries are, therefore, important. Unfortunately, the system is far too complex to allow detailed characterization of the isomerization reaction coordinate. The rate-limiting barrier must lie between the ortho ring complex and the hydrogen-bonded geometry, i.e., probably at geometries where ND<sub>3</sub> is interacting with the hydroxyl oxygen or ipso carbon (the atom to which OH is attached). To give a crude idea of the interactions experienced in such geometries, Table III, summarizes a series of single point MP2/6-31G\* calculations in which ND<sub>3</sub> was positioned in various orientations with respect to PhOH<sup>+</sup> at intermolecular separations of either 2 or 2.3 Å. Note that 2.3 Å is approximately the equilibrium intermolecular separation in the ring-bound complexes (B and C, Fig. 1). In these calculations, the PhOH<sup>+</sup> and ND<sub>3</sub> substructures

were frozen in the geometries found in the [PhOH-ND<sub>3</sub>]<sup>+</sup> hydrogen-bonded complex.

The first three geometries in the table have ND<sub>3</sub> positioned with its symmetry axis perpendicular to the PhOH plane, with the N atom 2 or 2.3 Å from the plane, and with its lone pair pointing at the hydroxyl H, O, or ipso-C atoms (“LP over H,” etc.). The “flipped over,” geometries are identical to the “LP over” geometries, except that the ND<sub>3</sub> is inverted. The in and out-of-plane “NH-O” geometries have the potential for ND-O hydrogen bonding, i.e., one ND bond in ND<sub>3</sub> is directed at the hydroxyl O atom, either in or perpendicular to the PhOH plane. Note that all geometries are repulsive with respect to reactants. For comparison, the final two structures are in the near-linear (PhOH-ND<sub>3</sub>) hydrogen-bonded geometry, but with the intermolecular separation stretched or stretched with the ND<sub>3</sub> rotated such that its symmetry axis is at 35° to the hydrogen bond axis. Note that these distorted hydrogen-bonded structures are attractive with respect to reactants.

Obviously, these frozen geometry calculations give only a crude picture of the potential. In particular, it is expected that the energy of the “LP over O” and “LP over H” geometries should be greatly lowered by allowing the hydroxyl H to relax into a position in between the nitrogen and oxygen atoms, developing some hydrogen bond character. For example, in the LP over O geometry, moving the hydroxyl H atom in between the O and N lowers the energy by at least 0.32 eV, although at that point the geometry is still repulsive with respect to reactants. It is less likely that hydroxyl geometry relaxation can significantly lower the energy in ND<sub>3</sub> on ipso C interactions. Clearly some of these geometries must become weakly attractive at larger ND<sub>3</sub>-PhOH<sup>+</sup> separations, but at long range the attraction is necessarily weak. The tentative conclusion from these calculations is that there is a significant barrier or barriers separating the ring-bound and hydrogen-bonded geometries.

With this scenario in mind, it is not surprising that H/D exchange should be so strongly inhibited by collision energy (a factor of 100 inhibition from a factor of 10 increase in  $E_{\text{collision}}$ ). Exchange requires a hydrogen-bonded complex that survives long enough for the necessary rearrangements. At high energies, such complexes presumably form only in the small fraction of collisions where the approach geometry is near-optimal, and even then the lifetime is too short (Table II) to result in efficient H/D scrambling. The short complex lifetime presumably also accounts for the observed, incomplete energy randomization. As collision energy is reduced, the first significant effects are probably that direct trapping into the hydrogen-bonded complex becomes more efficient, and that the complex lifetime increases, both factors enhancing the net H/D efficiency. At lower energies an increasing fraction of the H/D exchange signal arises from collisions that trap into ring-bound “precursor” complexes, and subsequently isomerize into hydrogen-bonded complexes where exchange can occur. In this mechanism, the net H/D exchange efficiency at low collision energies might be limited either by the efficiency with which ring-bound complexes form, or by the probability for transition from ring-bound to

hydrogen-bonded geometries, or by some combination of the two factors.

Given that the binding energies of the ring-bound complexes are more than a factor of 15 times our lowest collision energy, and that there are ten vibrations of the complex below  $500\text{ cm}^{-1}$ , intuition suggests that trapping into ring bonded complexes should be quite efficient at low energies. In that case, the  $\sim 50\%$  net reaction efficiency (some attributable to direct “ND<sub>3</sub> on hydroxyl” collisions) would have to be attributed to inefficient isomerization from ring to hydrogen-bonded complexes. In the statistical limit, the isomerization efficiency would be determined by the relative rates of isomerization and dissociation back to reactants. While we have no details about the isomerization transition state (or states), it is clear that this TS must be lower in energy and somewhat tighter than the orbiting transition state for dissociation of the complex. In that case, we expect that isomerization would be favored at low energies, with the fraction dissociating back to reactants increasing with energy. The predicted trend is, at least qualitatively, consistent with the experimental energy dependence.

For reference, the lifetime of the most strongly bound of the ring complexes (C in Fig. 1) ranges from  $\sim 2\text{ ns}$  for  $E_{\text{collision}} = 0.1\text{ eV}$ , to less than  $100\text{ fs}$  at  $E_{\text{collision}} > 1\text{ eV}$  (Table II). Note that these lifetimes neglect both interconversion between ring-bound complexes, and isomerization to the hydrogen-bonded geometry (and on to products). Interconversion will tend to lengthen the lifetime of the precursor(s) by pooling their density of states, but the effect should be no more than a factor of 2 because the para complex is the most stable of the ring-bound set. Isomerization to the hydrogen-bonded geometry will tend shorten the precursor lifetime by providing an additional decay channel, but this effect will also be at most a factor of 2, as the total efficiency of hydrogen-bonded complex formation is  $\leq 50\%$ .

Having isomerization as the rate-limiting step can also rationalize the substantial increase in low-energy H/D exchange efficiency upon ring-deuteration. Deuteration increases the density of states in the ring-bound complex by a factor ranging from 3.8 to 5 for collision energies from 0.1 to 0.5 eV. Because the affected vibrations are less active in the orbiting TS for dissociation, the sum of states at the TS increases by only a factor of 2%–30% over the same energy range, resulting in a net increase in lifetime by a factor of  $\sim 3.6$ , approximately independent of  $E_{\text{collision}}$ . Because the TS for isomerization is lower in energy than the orbiting TS for dissociation, ring deuteration should have a larger effect on the sum of states controlling isomerization. In that case, we would expect ring deuteration to enhance the probability for isomerization from ring to hydrogen-bonded complexes, consistent with observation.

The substantial vibrational enhancement of H/D exchange is not easily explained within a purely statistical mechanism. By invoking coupling of vibration to the reaction coordinate at the TS for isomerization, it is possible to rationalize the enhancement. Vibrational effects are discussed in the final section, below.

The alternative is to propose that the rate-limiting factor is the efficiency with which the ring-bound complexes form,

and that this efficiency is strongly inhibited by collision energy, and strongly enhanced by ring deuteration and vibration. Certainly, collision energy is expected to inhibit formation of the weakly bound complexes, though it is unclear whether the collision energy effect could be as strong as is observed. It also seems reasonable that ring deuteration should increase complex formation efficiency, by increasing the density of states in the complex. The higher density of states will tend to facilitate the collision-to-vibrational energy conversion required to form the complex. (As already noted, deuteration certainly increases the complex lifetime, as well.) Without detailed information about the collision dynamics, it is unclear whether this deuteration effect could be large enough to account for the near doubling of H/D exchange efficiency at low energies.

Finally, it is not obvious how one might account for the vibrational enhancement if the rate-limiting step were complex formation. Note that the vibrational effect is large enough that even at fixed collision energy, there is a substantial (factor of 2) increase in H/D exchange as energy is added in the form of vibration. Absent any dynamical effects, additional energy in the reactants would be expected to decrease complex formation.

Regardless of what factors control the contribution of precursor complexes to the H/D exchange mechanism, at some energy, the precursor is expected to become mechanistically insignificant. One crude measure of the significance of a complex is its lifetime, compared to some characteristic time associated with a direct collision (e.g., stripping or fast rebound collisions). In Table II, we compare complex lifetimes and the direct collision time, taken arbitrarily as the time required for relative motion by  $5\text{ \AA}$ . Note that the hydrogen-bonded complex lifetime is substantially greater than the direct collision time over most of the collision energy range where H/D exchange is significant. By this measure, the precursor complex is mechanistically significant at collision energies below  $\sim 0.8\text{ eV}$ . In particular, at low collision energies, formation of the precursor increases the collision time by orders of magnitude compared to a direct collision.

The precursor mechanism is also consistent with the substantial cross section observed for deeply inelastic, nonreactive scattering (Fig. 2), producing PhOH<sup>+</sup> with velocities near  $V_{\text{CM}}$ . There are three contributions to this signal. As noted, there is a  $\sim 20\%$  branching ratio for decay of the hydrogen-bonded complex back to reactants. This mechanism accounts for a substantial fraction ( $\sim 65\%$ ) of the nonreactive signal at the lowest collision energies, but by 0.5 eV formation of hydrogen-bonded complexes is inefficient (see above) and this channel accounts for less than 2% of the nonreactive signal. The major contribution over most of the experimental energy range will be collisions in the ND<sub>3</sub>-on-phenyl-ring geometry, and at low collision energies, many of these collisions will result in precursor complex formation. The nanosecond to picosecond lifetimes calculated for the precursor at  $E_{\text{collision}} \leq 0.6\text{ eV}$  are certainly sufficient to result in substantial collision-to-internal energy conversion, producing slow products with lab velocities near

$V_{CM}$ . At high collision energies, slow products must result from highly inelastic, but direct collisions.

### C. Proton transfer mechanism

As discussed elsewhere,<sup>11</sup> proton transfer (PT) was found to be endoergic, and as a consequence, is a minor product at low collision energies. We found that it was possible to fit the threshold behavior of the PT channel using either a line-of-centers model fit to the cross section, or a RRKM-based simulation of the branching fraction for PT products in dissociation of the hydrogen-bonded complex. These two fitting strategies are appropriate in opposite mechanistic limits. The line-of-centers model fit is predicated on the notion that reaction occurs in direct collisions, where the endoergicity is overcome by impulsive energy transfer. The RRKM branching model is appropriate for a mechanism where PT is simply one channel for decay of a statistical hydrogen-bonded complex. Both models lead to the same endoergicity ( $0.19 \pm 0.04$  eV). Our experiment leads to a neutral phenol OH bond energy that is within experimental error of the recent value from Ervin and co-workers<sup>20</sup> based on negative ion chemistry, but significantly larger than the earlier literature value.<sup>21</sup>

The congruence of the two limiting-case models raises the question of where the PT mechanism lies on the direct-statistical continuum, and how it relates to the mechanism for H/D exchange. Experiments with *d*<sub>5</sub>-PhOH indicate that only the hydroxyl proton is involved in either PT or H/D exchange. Because the hydroxyl proton is transferred, and there is a deep potential well for the hydrogen-bonded complex, one might think that most PT products form via a long-lived intermediate, at least at low collision energies. Figure 7 and Table I summarize the recoil velocity results for the PT product. Table II summarizes direct collision times and RRKM lifetimes for hydrogen-bonded and nonhydrogen-bonded complexes.

At  $E_{\text{collision}} = 1.5$  eV, the velocity distribution is backward peaked, indicating a collision time shorter than  $\sim 0.3$  ps. While longer than the direct collision time at this energy, 0.3 ps is substantially shorter than the lifetime for the hydrogen-bonded complex, indicating that most PT products do not result from breakup of a statistical, hydrogen-bonded complex. Further evidence for the nonstatistical nature of the PT channel comes from the recoil energy distribution. At  $E_{\text{collision}} = 1.5$  eV, the fraction of available energy appearing as recoil,  $\langle E_{\text{recoil}} \rangle / \langle E_{\text{avail}} \rangle$ , is 37%—significantly higher than would be expected for decay of a statistical complex.

As the collision energy is lowered, the velocity distributions become forward-backward symmetric within experimental error. Change to symmetric distributions at low  $E_{\text{collision}}$  is often the sign of a transition to a complex-mediated reaction mechanism, and such a transition would not be surprising in this system, given the substantial hydrogen bond energy. There are two observations that are inconsistent with a fully statistical mechanism, however. First, the fraction of available energy going into recoil ( $\langle E_{\text{recoil}} \rangle / \langle E_{\text{avail}} \rangle$ ) remains high as collision energy is decreased. Even at  $E_{\text{collision}} = 0.5$  eV, there is roughly four times the energy in

recoil expected for statistical decay (compare to the results for the H/D exchange channel, which is statistical at low energies). Note that it is possible to have high recoil energies in decay of a statistical complex, if there is a barrier in the exit channel that accelerates the products as they leave the transition state. The exit channel in the PT reaction has no such barrier.<sup>11</sup>

The other observation suggesting a nonstatistical PT mechanism comes from the RRKM-based modeling of the PT branching ratio.<sup>11</sup> RRKM theory was used to calculate the branching to PT vs energy in decay of the hydrogen-bonded complex. This RRKM branching was then convoluted with experimental broadening factors and compared with the experimental branching ratio. It was found that the RRKM simulation could fit the energy dependence of the experimental branching, but only if scaled by a factor of 10.2. The conclusion from the fitting is that decomposition of a statistical, hydrogen-bonded complex is only a minor contributor to the PT mechanism, even at low collision energies. This conclusion is consistent with the observed high recoil energies for the PT products.

The idea that PT is predominantly not statistical, even at low energies, seems surprising in light of the deep well associated with hydrogen bonding, and with the observed forward-backward symmetric velocity distributions. We propose the following mechanism. Roughly 10% of PT at low energies does, undoubtedly, originate in statistical decay of  $[\text{PhOHND}_3]^+$ . The balance must result from collisions that access the “ND<sub>3</sub> on hydroxyl” region of the potential surface, allowing transfer of the hydroxyl proton, but which separate to products without trapping into the hydrogen-bonded well long enough to randomize energy. The observation that PT is inefficient, even at energies well above threshold, is evidence that such collisions are rare.

“ND<sub>3</sub> on hydroxyl” geometries can be accessed both by collisions directly in this geometry, or as proposed above, by rearrangement from ring-bound precursor complexes. The relative importance of the two mechanisms is expected to be collision energy-dependent. At low energies the precursor mechanism is efficient, “delivering” a substantial fraction of collisions into “ND<sub>3</sub> on hydroxyl” geometries. At low energies, most of these collisions will ultimately trap into the deep hydrogen-bonded well, and as a consequence, the fraction of collisions leading to PT products is small. As energy is increased, the probability for trapping into the hydrogen-bonded well decreases, but so does the efficiency of the precursor mechanism. As a consequence, a smaller number of collisions access “ND<sub>3</sub> on hydroxyl” geometries, but a greater fraction of them go on to PT products. At energies above  $\sim 1$  eV, the precursor mechanism is inactive and most PT results from the relatively infrequent, direct “ND<sub>3</sub> on hydroxyl” collisions. At high energies, trapping into the hydrogen-bonded complex is also less efficient, thus PT occurs in a substantial fraction of “ND<sub>3</sub> on hydroxyl” collisions. The result of the competing mechanisms is a small, but nearly energy-independent cross section for PT.

#### D. Vibrational effects

The most surprising feature of this system, and the hardest to explain, is the large effect of low frequency ring vibrations. The modes excited (Fig. 1) have no obvious connection to the reaction coordinate, and little effect on the total energy of the system, particularly in comparison to the deep potential wells accessible to the reactants. Other than our recent report on reaction of  $\text{PhOH}^+$  with methylamine,<sup>3</sup> there are no vibrationally resolved studies of comparable systems to guide interpretation.

Some vibrational effects are easily understood. The energy dependence of the adduct cross section (Fig. 5, bottom) is mostly determined by the adduct lifetime, which should depend only on total energy. There are secondary effects that complicate matters, however. For example, only the hydrogen-bonded complex lives long enough to account for adduct detection (Table II), but the results for H/D exchange suggest that formation of such complexes is probably vibrationally enhanced via the precursor mechanism. On the other hand, for given total energy  $V_{\text{CM}}$  is lower for vibrationally excited reactants, increasing the flight time to the detector and possibly changing the collisional stabilization probability. Within these uncertainties, we would expect the adduct signal to depend largely on total energy, as is observed.

The proton transfer cross section at energies below 0.5 eV is, within the rather large experimental uncertainty, also dependent only on total energy. For an endoergic reaction near threshold, it is not unexpected that total energy might be the determining factor,<sup>22,23</sup> although in some such cases there are large mode-specific effects if a particular mode couples especially well to the reaction coordinate.<sup>24,25</sup> In this system, PT probably is occurring by at least two mechanisms in this energy range, making prediction of the expected vibrational effects difficult. At high collision energies, both  $\nu_{6a}$  and  $\nu_{12}$  excitations have a small, but reproducible, inhibitory effect. It is interesting to note that in proton transfer from  $\text{PhOH}^+$  to methylamine,<sup>3</sup> where the cross section is large enough to give good signal/noise, we observe vibrational effects qualitatively similar to those observed for  $\text{ND}_3$ . In the methylamine reaction there is a nonspecific effect from both vibrations and collision energy at low total energies, while at  $E_{\text{collision}} > 0.5$  eV, there is little effect of collision energy, but both vibrations inhibit proton transfer. The similarity is surprising in that PT from  $\text{PhOH}^+$  to  $\text{ND}_3$  is a minor channel, endoergic by 0.19 eV, while PT from  $\text{PhOH}^+$  to  $\text{CH}_3\text{NH}_2$  is the dominant channel in that system and exoergic by 0.44 eV.

It is interesting that the ring vibrations should slightly inhibit PT at high energies, where the vibrational energy is clearly insignificant. Particularly in the higher end of this energy range, the precursor mechanism is negligible and most PT must occur in collisions directly in “ $\text{ND}_3$  on hydroxyl” geometries, where the proton is transferred and the products separate without trapping into a statistical complex. The vibrational inhibition could result either from vibrational inhibition of the proton transfer probability, or from a vibrationally enhanced probability of trapping into the statistical complex. If the latter were true, then the H/D exchange cross section should also be vibrationally enhanced at high ener-

gies, in contrast to experiment (note change of energy scales in Fig. 5). The tentative conclusion is that these vibrations, which both involve significant motion of the OH group as a unit, somehow inhibit attack on the hydroxyl proton by  $\text{ND}_3$ .

The classical periods of the  $\nu_{6a}$  and  $\nu_{12}$  vibrations are 65 and 40 fs, respectively, and the root mean square atomic displacement is 0.025 Å, with maximum displacements around 0.04 Å. In the 0.5–2.5 eV collision energy range where the inhibition is observed, the relative motion time scale ranges from  $\sim 40$  fs/Å to  $\sim 25$  fs/Å, i.e., the vibrational period is comparable to the time for relative motion over a bond length. Note, however, that the atomic velocities resulting from vibration are much smaller than velocities resulting from relative motion of the reactants. Based on this consideration, it appears that the explanation for the vibrational effect at high energies must invoke some vibration-induced change in the reactant properties, rather than some effect of the vibrational motion itself.

One possibility is vibration-induced changes in electronic structure that might influence bonding or long-range electrostatic interactions. We calculated orbital populations, atomic charges (Mulliken and CHelpG), and total electron density for  $\text{PhOH}^+$  in its equilibrium structure, and for distortions along  $\nu_{6a}$  and  $\nu_{12}$  normal coordinates roughly equal to the classical vibrational amplitudes. Using gOpenMol (Ref. 14) to visualize electron density surfaces with various cutoff densities, there are no apparent changes in the shape of the electron cloud. The average variation in atomic charge (CHelpG) as  $\text{PhOH}^+$  vibrates is  $\sim 0.01$ , and the root mean square variation is less than 0.02. The largest variation is for one of the meta carbon atoms (0.05), but the ipso carbon, and hydroxyl O and H atoms show charge variations less than 0.01. We also considered the extent to which the moving atoms might change the center-of-charge or dipole moment of  $\text{PhOH}^+$ . The center-of-charge moves by about 0.035 Å between the vibrational extrema of  $\nu_{6a}$ , and by only 0.011 Å for  $\nu_{12}$ . The magnitude of the dipole moment changes by less than 3% for either vibration, and the direction also is nearly constant. It seems unlikely that such small changes in electrostatic properties could have a significant effect on the long-range interaction of  $\text{ND}_3$  with  $\text{PhOH}^+$ , but small effects on the short range dynamics controlling PT cannot be excluded.

The other obvious possibility is that the effect is geometrical, i.e., steric. In this case, the relevant parameters are the distance separating the hydroxyl proton from neighboring atoms that might block access. The equilibrium distance between the hydroxyl H and the hydrogen attached to the ortho carbon atom is 2.35 Å, and this distance varies from  $\sim 2.3$  to  $\sim 2.4$  Å during either vibration. Here, again, the vibrationally-induced changes are small, but could possibly result in a small change in the PT efficiency at high energies.

The largest effect is the substantial ( $>2$  times) vibrational enhancement of H/D exchange at low collision energies. It is certain that in the statistical hydrogen-bonded complex where H/D exchange occurs, any memory of the reactant energy partitioning is lost, and the vibrational effect must result from some event earlier along the reaction coordinate. We have argued that the dominant contribution to

H/D exchange at low energy involves a ring-bound precursor complex, and that the vibrational effect is manifest either as a vibrational enhancement of complex formation, or as vibrational enhancement of the ring-to-hydrogen-bonded isomerization.

The notion that ring vibration somehow greatly enhances the probability for formation of ring-bound complexes is difficult to support. Certainly it would not be surprising to find a modest enhancement resulting from partitioning energy from collision energy to vibration at constant total energy (Fig. 5). Note, however, that there is a substantial (factor of 2) enhancement even from adding vibrational energy at constant collision energy, and it is difficult to see how adding to the total energy of the colliding partners could enhance the probability of trapping into a weakly-bound complex. Such an effect would require a dynamical explanation that would require strong coupling between the PhOH<sup>+</sup> ring vibrations and the relative motion of the two reactants. As discussed below, the coupling, in fact, appears to be rather weak.

The other avenue for a vibrational enhancement is vibrationally enhanced isomerization from ring to hydrogen-bonded geometries. This possibility would require that the initial vibrational state not be immediately scrambled in forming the ring complex, and there is some precedent for such vibrational adiabaticity. In reaction of C<sub>2</sub>H<sub>2</sub><sup>+</sup> with methane, for example, C<sub>2</sub>H<sub>2</sub><sup>+</sup> bending vibration substantially enhances the endoergic H atom abstraction reaction, while the CC stretch has little effect.<sup>25</sup> In a paper reporting *ab initio* calculations and transition state theory on this reaction, Klippenstein<sup>26</sup> proposed that the absence of a CC stretch effect results from weak coupling of this mode in a precursor complex. As a consequence, the reaction was proposed to be adiabatic in the CC stretch mode, so that its vibrational energy is not available to drive the endoergic reaction.

The situation for the ring-to-hydrogen-bonded isomerization process is somewhat different. Isomerization is exoergic, its limiting TS is certainly below the energy of the orbiting TS for dissociation, and we are trying to explain a larger-than-expected vibrational effect, not absence of an effect. Nonetheless, with the addition of some dynamics, vibrational adiabaticity may explain our results. Suppose that the ring vibrations are adiabatic in the ring-complex, and thus are not available to promote dissociation. They may, on the other hand, couple strongly as the system approaches the isomerization TS, thus making the vibrational energy available to drive isomerization. Of course, if isomerization fails to occur at this point, then the ring vibrational energy will be available to drive dissociation of the ring complex. If, however, the coupling occurs only at geometries near the isomerization TS, there may be a high probability for vibrationally driven isomerization. In essence, we argue that the in-plane ring vibrations may have little effect on formation of the ring-bound complex or on motion of ND<sub>3</sub> in the complex, but that as the ND<sub>3</sub> approaches the isomerization TS, vibrational coupling may help "push" ND<sub>3</sub> over the barrier. Certainly the vibrational motion of the hydroxyl O and ipso C atoms is in the direction needed to give a push along the isomerization coordinate.

For this scenario to be possible, we require weak cou-

pling in the complex, and strong coupling in the TS region. There are vibrations of the complex in which the motion of the PhOH<sup>+</sup> moiety is essentially identical to the  $\nu_{6a}$  and  $\nu_{12}$  vibrations of free PhOH<sup>+</sup>. Furthermore, in both vibrations of the complex, the ND<sub>3</sub> moiety is nearly stationary. As expected for such vibrations, the frequencies are also shifted very little from free PhOH<sup>+</sup>. The vibration corresponding to  $\nu_{6a}$  in free PhOH<sup>+</sup> is blue-shifted by  $\sim 3$  cm<sup>-1</sup> ( $\sim 0.5\%$ ) in the complex. The  $\nu_{12}$  vibration is also blue-shifted, but by only 0.5 cm<sup>-1</sup> (0.06%). The implication is that the two in-plane ring modes studied are, indeed, very weakly coupled to the ND<sub>3</sub> moiety.

It is almost certainly also the case that the ring vibrations couple strongly with ND<sub>3</sub> motion as the system approaches the TS for isomerization. This TS (or set of TSs) must be in a geometry corresponding to ND<sub>3</sub> interacting with the ipso carbon or hydroxyl oxygen atoms. As shown in Table III, the interaction potential in this region of configuration space is strongly dependent on the ND<sub>3</sub> position relative to these atoms. The motion of these atoms in the vibrations will, therefore, be strongly coupled to ND<sub>3</sub> motion. The coupling will certainly end any adiabaticity of these vibrations as the TS is approached, and may also provide a mechanism for vibrationally enhanced barrier crossing.

Certainly, we are far from being able to give a definitive explanation of the vibrational effects in this system. The surprising result is that large effects can exist for low frequency vibrations of such a large (and apparently statistical) system. We are optimistic that by probing vibrational effects on other reactions of benzenoid cations, and by examining the effects of other vibrations, we will be able to at least partly unravel the dynamics.

## ACKNOWLEDGMENTS

The authors would like to thank Alex Boldyrev, Jack Simons, and William Hase for helpful suggestions. This work was supported by the National Science Foundation under Grant No. CHE-9807625. We are also grateful for a grant of computer time from the Utah Center for High Performance Computing. The SGI Origin 2000 used was partly funded by the SGI Supercomputing Visualization Center Grant.

<sup>1</sup>S. L. Anderson, *Adv. Chem. Phys.* **82**, 177 (1992).

<sup>2</sup>S. L. Anderson, *Acc. Chem. Res.* **30**, 28 (1997).

<sup>3</sup>H.-T. Kim, R. J. Green, and S. L. Anderson, *J. Chem. Phys.* (in press).

<sup>4</sup>J. Qian, R. J. Green, and S. L. Anderson, *J. Chem. Phys.* **108**, 7173 (1998).

<sup>5</sup>H. Fu, J. Qian, R. J. Green, and S. L. Anderson, *J. Chem. Phys.* **108**, 2395 (1998).

<sup>6</sup>J. Qian, H. Fu, and S. L. Anderson, *J. Phys. Chem.* **101**, 6504 (1997).

<sup>7</sup>Y.-h. Chiu, H. Fu, J.-t. Huang, and S. L. Anderson, *J. Chem. Phys.* **102**, 1199 (1995).

<sup>8</sup>Y.-h. Chiu, H. Fu, J.-t. Huang, and S. L. Anderson, *J. Chem. Phys.* **105**, 3089 (1996).

<sup>9</sup>L. Zhu and P. Johnson, *J. Chem. Phys.* **94**, 5769 (1991).

<sup>10</sup>M. J. Frisch, G. W. Trucks, H. B. Schlegel, G. E. Scuseria, M. A. Robb, J. R. Cheeseman, V. G. Zakrzewski, J. A. Montgomery, R. E. Stratmann, J. C. Burant, S. Dapprich, J. M. Millam, A. D. Daniels, K. N. Kudin, M. C. Strain, O. Farkas, J. Tomasi, V. Barone, M. Cossi, R. Cammi, B. Menucci, C. Pomelli, C. Adamo, S. Clifford, J. Ochterski, G. A. Peterson, P. Y. Ayala, Q. Cui, K. Morokuma, D. K. Malick, A. D. Rabuck, K. Ragh-

- vachari, J. B. Foresman, J. Cioslowski, J. V. Ortiz, B. B. Stefanov, G. Liu, A. Liashenko, P. Piskorz, I. Komaromi, R. Gomperts, R. L. Martin, D. J. Fox, T. Keith, M. A. Al-Laham, C. Y. Peng, A. Nanayakkara, C. Gonzalez, M. Challacombe, P. M. W. Gill, B. G. Johnson, W. Chen, M. W. Wong, J. L. Andres, M. Head-Gordon, E. S. Replogle, and J. A. Pople, GAUSSIAN 98 (Gaussian, Inc., Pittsburgh, Pennsylvania, 1998).
- <sup>11</sup>H.-T. Kim, R. J. Green, J. Qian, and S. L. Anderson, *J. Chem. Phys.* **112**, 5717 (2000).
- <sup>12</sup>M. Yi and S. Scheiner, *Chem. Phys. Lett.* **262**, 567 (1996).
- <sup>13</sup>J. B. Foresman and A. Frisch, *Exploring Chemistry with Electronic Structure Methods*, 2nd ed. (Gaussian, Pittsburgh, 1993).
- <sup>14</sup>L. Laaksonen, 1.31 ed. (available at <http://laaksonen.csc.fi/gopenmol/gopenmol.html>, Espoo, Finland, 1999).
- <sup>15</sup>S. L. Anderson, L. Goodman, K. Krogh-Jespersen, A. G. Ozkabak, R. N. Zare, and C.-f. Zheng, *J. Chem. Phys.* **82**, 5329 (1985).
- <sup>16</sup>C. M. Breneman and K. M. Wiberg, *J. Comput. Chem.* **11**, 361 (1990).
- <sup>17</sup>J. Troe, *Chem. Phys. Lett.* **122**, 425 (1985).
- <sup>18</sup>G. A. Fisk, J. D. McDonald, and D. R. Herschbach, *Discuss. Faraday Soc.* **44**, 228 (1967).
- <sup>19</sup>L. Zhu and W. L. Hase, *Quant. Chem. Prog. Exchange*, QCPE 644.
- <sup>20</sup>V. F. DeTuri and K. M. Ervin, *Int. J. Mass Spectrom. Ion Processes* **175**, 123 (1998).
- <sup>21</sup>R. M. Borges dos Santos and J. A. Martinho Simoes, *J. Phys. Chem. Ref. Data* **27**, 707 (1998).
- <sup>22</sup>B. Yang, Y. H. Chiu, and S. L. Anderson, *J. Chem. Phys.* **94**, 6459 (1991).
- <sup>23</sup>B. Yang, Y. H. Chiu, H. Fu, and S. L. Anderson, *J. Chem. Phys.* **95**, 3275 (1991).
- <sup>24</sup>Y.-h. Chiu, B. Yang, H. Fu, S. L. Anderson, M. Schweizer, and D. Gerlich, *J. Chem. Phys.* **96**, 5781 (1992).
- <sup>25</sup>Y.-h. Chiu, H. Fu, J.-t. Huang, and S. L. Anderson, *J. Chem. Phys.* **101**, 5410 (1994).
- <sup>26</sup>S. J. Klippenstein, *J. Chem. Phys.* **104**, 5437 (1996).